Biochimica et Biophysica Acta 1788 (2009) 1976–1986

Contents lists available at ScienceDirect

Biochimica et Biophysica Acta

journal homepage: www.elsevier.com/locate/bbamem

Biophysical studies of the membrane location of the voltage-gated sensors in the HsapBK and KvAP K^+ channels

Henrik Biverståhl, Jesper Lind, Andrea Bodor [1], Lena Mäler *

Center for Biomembrane Research, Department of Biochemistry and Biophysics, The Arrhenius Laboratory, Stockholm University, Stockholm 10691, Sweden

ARTICLE INFO

Article history:
Received 20 April 2009
Received in revised form 30 June 2009
Accepted 1 July 2009
Available online 10 July 2009

Keywords:
K^+-channel
Voltage-sensor
Membrane
Bicelle
Micelle
NMR
Fluorescence

ABSTRACT

The membrane location of two fragments in two different K^+-channels, the KvAP (from *Aeropyrum pernix*) and the HsapBK (human) corresponding to the putative "paddle" domains, has been investigated by CD, fluorescence and NMR spectroscopy. Both domains interact with $q = 0.5$ phospholipid bicelles, DHPC micelles and with POPC vesicles. CD spectra demonstrate that both peptides become largely helical in the presence of phospholipid bicelles. Fluorescence quenching studies using soluble acrylamide or lipid-attached doxyl-groups show that the arginine-rich domains are located within the bilayered region in phospholipid bicelles. Nuclear magnetic relaxation parameters, T_1 and ^{13}C–^1H NOE, for DMPC in DMPC/DHPC bicelles and for DHPC in micelles showed that the lipid acyl chains in the bicelles become less flexible in the presence of either of the fragments. An even more pronounced effect is seen on the glycerol carbons. ^2H NMR spectra of magnetically aligned bicelles showed that the peptide derived from KvAP had no or little effect on bilayer order, while the peptide derived from HsapBK had the effect of lowering the order of the bilayer. The present study demonstrates that the fragments derived from the full-length proteins interact with the bilayered interior of model membranes, and that they affect both the local mobility and lipid order of model membrane systems.

1. Introduction

Voltage-gated potassium channels (Kv) open and close due to the motion of the voltage-sensor domain in response to changes in the transmembrane potential. During this movement, the transmembrane domain embedded in the lipid bilayer is believed to undergo conformational changes associated with displacement of the charged amino acids, usually Arg residues [1–3].

Structurally, the Kv channels are homotetramers in which each subunit contains six transmembrane helices, named S1–S6. The crystal structure of the open form of the Kv channel has revealed that it contains a central ion-conducting pore (S5–S6) surrounded by voltage sensors (S1–S4) [4–8]. Certain charged amino acids within the voltage sensors, particularly the Arg residues in S4, account for most of the gating charge. The S4 segment forms, together with a part of the S3 helix, S3b, a domain known as the "paddle" domain or the "arginine-rich paddle" [5]. This helix-turn-helix motif is attached to the rest of the domain by flexible hinges and is believed to move in response to membrane voltage changes [3]. This movement causes the Kv channel to be open or closed depending on the electrochemical potential over the cell membrane. Both experimental and bioinformatic studies have shown that this voltage sensor is conserved in a wide range of voltage dependent channels [9–11]. It has also been demonstrated that the voltage sensor motif can function on its own as a voltage-activated proton channel without a separate pore domain [10,11] and that the paddle domain in Kv and Nav channels is modular and can be swapped between different ion channels [12–14]. The "paddle" domain model and its movement are, however, controversial. Different biophysical and biochemical techniques have been shown to give different results concerning the actual distance that the domain moves [8,15,16].

To study details of the membrane interaction, we investigated the position of two putative S3b–S4 domains from two different potassium channels, KvAP and HsapBK in different model membranes. The KvAP channel is from the thermophilic archaebacteria *Aeropyrum pernix* while the HsapBK channel is the Human calcium and voltage-activated BK channel. The structure of BK channels (also known as Maxi-K channels) differs from Kv channels in two major ways; BK channels have seven transmembrane segments (S0–S6) and a cytosolic Ca^{2+}-activation region (S7–S10) [17]. The Ca^{2+}-activation and the voltage activation act independently of each other. A recent NMR-derived solution structure of the "paddle" domain from HsapBK showed that this part adopts a helix-turn-helix conformation, which further supports the modular nature of the S3b–S4 part of the channel [18].

The KvAP fragment that corresponds to the S3b–S4 domain contains 35 amino acids (hereafter called KvAPp) and it is derived

Abbreviations: NMR, nuclear magnetic resonance; CD, circular dichroism; NOE, nuclear Overhauser enhancement; DHPC, 1,2-dihexanoyl-*sn*-glycero-3-phosphatidylcholine; DMPC, 1,2-dimyristoyl-*sn*-glycero-3-phosphatidylcholine; POPC, 1-palmitoyl-2-oleoyl-phosphatidylcholine

* Corresponding author. Tel.: +46 8 162448; fax +46 8 155597.
E-mail address: lena.maler@dbb.su.se (L. Mäler).
[1] Present address: Eötvös University, Institute of Chemistry, Laboratory of Structural Chemistry and Biology, Budapest 1117, Hungary.

0005-2736/$ – see front matter © 2009 Elsevier B.V. All rights reserved.
doi:10.1016/j.bbamem.2009.07.001

from residues 99 through 133 in the full-length protein (Table 1). In order to investigate the position of the domain in model membranes by Trp fluorescence experiments, we also use a mutant where the Phe18 was substituted for a Trp (F18W-KvAPp). The corresponding S3b–S4 domain in HsapBK, derived from residues 233 through 260 in the full-length protein (HsapBKp), consists of 28 amino acid residues (Table 1).

Peptide positioning in model membranes can be investigated in numerous ways. Studies can be conducted either on the peptide or on the lipids within the model membrane, and two of the most commonly used methods are fluorescence and NMR spectroscopy.

Fluorescence studies conducted on the peptides are based on changes in the Trp wavelength of the peptide, that aid in monitoring protein folding, and membrane interaction [19]. Fluorescence intensities can also be measured in the presence and absence of a quenching agent, such as acrylamide or doxyl-labeled lipid, to give information about the location of the peptide in a bilayer.

There are several NMR methods for elucidating the effect of peptides on membrane mobility and order [20–26]. ^{31}P NMR as well as ^{2}H NMR has been used to determine the phase properties of lipid mixtures, including bicelles [27,28], and the effect of bioactive peptides on lipid bilayers. ^{13}C–^{1}H dipolar couplings [29,30] of phospholipids of ordered bilayers or bicelles have been reported. The effect of an antimicrobial model peptide and of a lipophilic drug on bicelle order and structure has recently been determined [30,31] by the use of ^{13}C–^{1}H dipolar coupling in magnetically aligned bicelles and more recently bicelles have been used in solid-state NMR investigations of cytochrome P450 and b_5 [32,33] and of Islet amyloid polypeptide [34].

Spin relaxation has previously been used successfully to investigate effects of peptides and protein fragments on lipid dynamics. The DMPC dynamics in bicelles [35–37] have previously been determined and it was shown that the lipid dynamics in the bicelle agree well with the dynamics in unilamellar vesicles obtained from EPR methods [38,39] as well as from NMR spin relaxation [40,41].

Most investigations of peptide-bilayer interactions have been made using phospholipid vesicles. Bicelles, composed of mixtures of phospholipid and a detergent [42–49], however, provide a convenient way of conducting high-resolution NMR studies of both the bound peptide and of lipid properties. Recently we reported a carbon-13 relaxation study of the interaction between the lytic peptide melittin in small, fast-tumbling bicelles [36] and between model transmembrane peptides and bicelles [37]. Melittin has previously been extensively studied, using a multitude of biophysical techniques, with respect to its structure, dynamics and membrane interactions, including membrane perturbing effects [50–56]. The relaxation study in bicelles showed that natural abundance carbon-13 relaxation is a useful tool for investigating lipid reorientation and the effect of membrane-interacting peptides on lipid dynamics.

In this study, we have investigated the location of the domains, and the influence of the fragments on lipid order and dynamics by several techniques, including fluorescence and NMR spin relaxation. The results in the present investigation show that the two K^+-channel fragments are located within the lipid bilayer of various membrane mimetic media. More interestingly, the results also show that the peptides have different effects on the mobility and order of the lipids in the model membranes.

Table 1
Details for peptides used in the present study.

Peptide	Sequence	Net charge
KvAPp	PAGLLALIEGHLAGLGLFRLVRLLRFLRILLIISR	+5
F18W-KvAPp	PAGLLALIEGHLAGLGLWRLVRLLRFLRILLIISR	+5
HsapBKp	PVFVSVYLNRSWLGLRFLRALRLIQFSE	+4

2. Materials and methods

2.1. Materials

Phospholipids, 1-palmitoyl-2-oleoyl-phosphatidylcholine (POPC), dihexanoyl-sn-glycero-3-phosphatidylcholine (DHPC), dimyristoyl-sn-glycero-3-phosphatidylcholine (DMPC), as well as d_{22}-DHPC and d_{54}-DMPC, and 5-, 12- and 16-doxyl-labeled POPC were obtained from Avanti Lipids Inc. (Alabaster, AL, USA). The peptides KvAPp, F18W-KvAPp and HsapBKp were obtained from group SNPE (Strasbourg, France) and they were used without further purification. The purity of the peptides (as judged from HPLC analysis) was at least 85%. Mass spectrometry analysis yielded a molecular weight of 3894 Da for KvAPp (theoretical mass 3894 Da), 3932 Da for F18W-KvAPp (theoretical mass 3933 Da) and 3380 for HsapBKp (theoretical mass 3380).

2.2. Preparation of vesicles

POPC lipids were dissolved in a mixture of chloroform and methanol (65:25) together with the peptide (KvAPp, F18W-KvAPp or HsapBKp) at a lipid to peptide ratio of 100. The residual solvent was removed by placing the sample under a flow of N_2 gas until the lipids were dry. To ensure that no solvent remained the lipid/peptide sample was put in a freeze-dryer for at least 1 h. The dried lipid/peptide film was then dissolved in 50 mM potassium phosphate (KPi) buffer, pH 7.4, to obtain a lipid concentration of 10–20 mM. The solution was vortexed to form large multilamellar vesicles (LMVs). Then the LMVs were freeze-thawed using liquid nitrogen/40 °C water bath, which results in a decreased lamellarity. The sample was repeatedly extruded about 20 times through polycarbonate microfilters with 100 nm pores to obtain a uniform sample of large unilamellar vesicles (LUVs), with a diameter of 100 nm [57]. Vesicles of this size have an inner volume of around 10^{-18} L, which means that the bulk solution is outside the vesicles. The vesicle solution was diluted to a final concentration of 1–5 mM lipids.

2.3. Preparation of bicelle and DHPC micelle samples

DHPC/DMPC bicelle samples with $q = 0.5$ [27,45] were prepared using a stock solution of DHPC, which was added to a slurry of DMPC in water. The mixture was vortexed until a clear, non-viscous, solution was formed. The final concentration of the sample was 200 mM DHPC, 100 mM DMPC, 50 mM phosphate buffer (pH 7.4). Samples containing KvAPp, F18W-KvAPp or HsapBKp were produced by adding an amount of peptide corresponding to a concentration of 0.5 or 3 mM to the ready-made bicelle solution followed by vortexing. Ten percent D_2O was used in the NMR samples for field/frequency lock stabilization. For carbon-13 relaxation measurements on DMPC, chain-perdeuterated DHPC (d_{22}-DHPC) was used. Samples containing 3 mM peptide in DHPC micelles were produced by dissolving the peptide in 200 mM DHPC.

Spin-labeled lipids were dissolved in methanol, and this solution was added in small amounts to the ready-made bicelles (typically 2.5 to 25 μL solution to a sample of 600 μL), and the sample was then rapidly vortexed for about 1 min. This procedure has been used successfully for NMR investigations of paramagnetic effects both in micelles [58,59] and bicelles [60,61], and no effect of the small amount of methanol has been observed on micelle or bicelle morphology. The concentration of spin-labeled lipids in the samples was between 50 and 200 μM.

Magnetically aligned bicelles were prepared in the same way as described for the $q = 0.5$ bicelles, but with $q = 3.5$. In this case chain-perdeuterated DMPC (d_{54}-DMPC) was used. A small residual $^{2}H_2O$ signal was visible in the NMR spectra, even if ^{2}H-depleted H_2O was used. Also, in this case, several freeze-thaw cycles were employed

until a clear solution was obtained at room temperature. Peptide was then added to the ready-made bicelle solution to yield a concentration of 3 mM. Once in the spectrometer, the temperature was cycled between below the gel–liquid crystal transition temperature and above the induction of the ordered phase (between 10 and 45 °C).

2.4. CD spectroscopy

Far-UV CD measurements were made on an Applied photophysics chirascan CD spectropolarimeter (Surrey, United Kingdom) with a 50 μm quartz cuvette. Wavelengths ranging between 190 and 250 nm were scanned, with a 0.5 nm step resolution and 100 nm/min scan speed. The response time was 4 s, with 50 mdeg sensitivity and a 1 nm band width. Measurements were conducted at 37 °C and the temperature was controlled by a quantum northwest TC 125 temperature controller. Spectra were collected and averaged over 1–10 scans. The CD spectra were evaluated using Applied photophysics Pro-Data viewer v 4.0.17.

2.5. Dynamic Light Scattering

The size of DHPC micelles was measured by performing dynamic light scattering experiments on 30 mM and 75 mM DHPC dissolved in H_2O. DLS measurements were recorded on a Zetasizer instrument (Nano ZS, Malvern Instruments, Worcestershire, United Kingdom) with a glass cuvette of 1 cm path length. Scattering data were collected during 10 s with an accumulation over 10 scans and presented as autocorrelation functions. Measurements were performed in the temperature interval 20–40 °C. All experiments were repeated 8 times and equilibrated 15 min between every temperature step. The data were processed with the manufacturer software (DTS) and presented as scattering intensity autocorrelation decays. The Stoke–Einstein relationship, together with refractive indices provided by the software and temperature corrected viscosities, was used to calculate the hydrodynamic diameter of the detergent aggregates.

2.6. Fluorescence spectroscopy

All fluorescence spectroscopy measurements were carried out using a Fluorolog 3 spectrometer (Jobin Yvon Horiba Inc.) and analyzed with the Datamax software (version 2.20). All measurements were done at 25 or 37 C using a 2×10 mm quartz cuvette. The excitation wavelength was 280 nm and the emission was scanned from 300 to 450 nm. Scans were taken with 1 nm excitation and emission bandwidths, at a scan speed of 300–600 nm/min. Fluorescence was measured for samples containing $q=0.5$ DMPC/DHPC bicelles (300 mM total lipid) with 1.5 mM peptide and for samples containing POPC vesicles (1–5 mM) and 10–50 μM peptide. The effect on fluorescence signal intensity of the hydrophilic quencher acrylamide and of POPC labeled with a doxyl group attached to position 5, 12 or 16 in the acyl chain was monitored as a function of quencher concentration.

Quenching constants, K_{SV}, were estimated from a linear regression with the Stern-Volmer equation [19]:

$$\frac{F_0}{F} = 1 + K_{SV}[Q] \tag{1}$$

where F and F_0 are the fluorescence intensities in the presence and absence of the quencher, respectively, and [Q] is the concentration of acrylamide.

2.7. NMR spectroscopy

NMR experiments were carried out on a Bruker Avance spectrometer (Bruker Biospin, Fällanden, Switzerland) operating at 9.39 T as well as on a Varian Inova (Palo Alto, CA) spectrometer operating at 14.09 T. Natural abundance ^{13}C R_1 relaxation measurements were performed with the standard inversion recovery pulse sequence (direct ^{13}C detection with WALTZ16 ^1H decoupling during the entire experiment), using 10 relaxation delays ranging from 0.01 to 10 s. The ^{13}C $\pi/2$ pulse length was around 12–14 μs on both spectrometers and a pre-acquisition delay of a minimum of 4 s was used. The T_1 parameters were evaluated using a three-parameter fit of the measured intensities. Errors were evaluated by recording two time-points twice. Steady-state NOE factors were measured by taking the ratio of intensities in a spectrum acquired with and without employing a long (27 s) ^1H irradiation prior to detecting on ^{13}C. Errors in the NOE factors were evaluated from duplicate experiments. The number of scans ranged from 400 to 512 in the R_1 measurements, and 800 to 1024 in the NOE measurements. Relaxation was measured for DMPC in $q=0.5$ DMPC/DHPC bicelles with and without 3 mM of either of the two peptides, and for DHPC in 200 mM DHPC with and without either of the two peptides. All relaxation experiments were recorded at 37 °C.

The ^2H NMR experiments were carried out at 61.4 MHz ^2H frequency (9.39 T) using a Bruker Avance spectrometer. The spectra were acquired with a double-resonance probe-head using the standard quadrupolar echo sequence $\pi/2$-τ_1-$\pi/2$-τ_2-acq [62] where $\tau_1=50$ μs and $\tau_2=40$ μs, and with a $\pi/2$ pulse width of 14 μs. The recycle delay between scans was 2 s and the spectral width was 100 kHz. Typically 30,000 to 40,000 transients were accumulated and data were collected at 37 °C. The FID was multiplied with an exponential function with a line-broadening of 10 Hz prior to Fourier transformation. The measured quadrupolar splittings (Δ) can be related to the segmental order parameter, S_{CD}, of the C–^2H bond. For a bicelle, aligned with its normal perpendicular to the static magnetic field this relation is given by

$$\Delta = \frac{3}{2}\left(\frac{e^2qQ}{h}\right)S_{CD}\left(\frac{1}{2}\right) \tag{2}$$

in which e^2qQ/h is the quadrupolar coupling constant (~168 kHz for an alkyl C–^2H bond) [20,21].

2.8. NMR relaxation data evaluation

For an isolated ^{13}C–^1H spin-pair, or for carbons carrying several equivalent protons, which can be assumed for natural abundance ^{13}C, the relaxation is dominated by the dipole–dipole interaction between the two nuclei. The relaxation rates for each individual ^{13}C–^1H spin-pair are given by

$$R_1 = \frac{d^2}{4}[J(\omega_H - \omega_C) + 3J(\omega_C) + 6J(\omega_H + \omega_C)] \tag{3}$$

$$\mathrm{NOE} = 1 + \frac{d^2\gamma_H}{4R_1\gamma_C}(6J(\omega_H + \omega_C) - J(\omega_H - \omega_C)) \tag{4}$$

in which d is the dipole–dipole interaction strength constant given by $d=(\mu_0/4\pi)\gamma_H\gamma_C\hbar r_{CH}^{-3}$. The number of protons on each carbon is given by n and r_{CH} is the inter-nuclear distance, set to 1.1 Å. The CSA contribution to the relaxation was assumed to be zero.

To model the lipid dynamics in a bicelle, we used an extension of the classical model-free approach [40,41,63–68]. Several degrees of motional freedom must be considered for a lipid molecule in a bilayer. A lipid molecule in a membrane is free to rotate around its principal axis but the rotation around the other two axes is strongly restricted by the membrane surface. In order to accurately describe its motion, an order parameter and correlation time for the entire lipid molecule, S^2_{lipid} and τ_{lipid}, is required (see Fig. 1 for an illustration of the lipid dynamics). This concept is the same for the local motion. In principle,

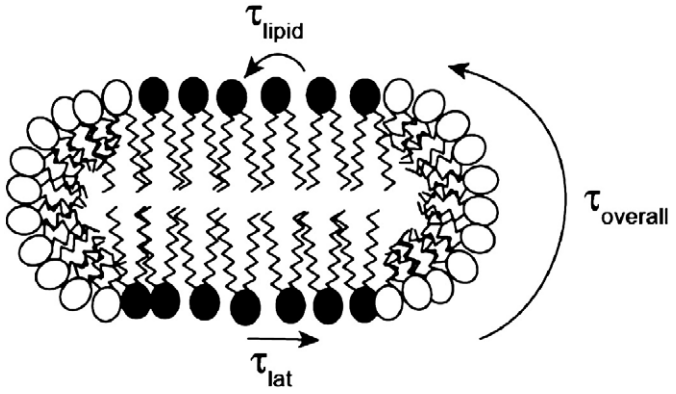

Fig. 1. Schematic illustration of the different motions (in terms of correlation times) used for evaluating the lipid carbon-13 relaxation data for DMPC in bicelles and for DHPC in micelles. The head-groups in DHPC molecules are indicated by open symbols, while head-groups in DMPC molecules are indicated by filled symbols.

one needs also to consider the overall tumbling of the entire bicelle aggregate. The predicted correlation time for an aggregate of the size of the bicelles used here is, however, far too large to affect the spectral density and can thus safely be neglected in the evaluation of R_1 and NOE data [68]. Accepting these assumptions, a minimal spectral density function, given by

$$J(\omega) = \frac{2}{5}\left[\frac{\left(S^2_{local} - S^2_{local}S^2_{lipid}\right)\tau_{lipid}}{1+\omega^2\tau^2_{lipid}} + \frac{\left(1-S^2_{local}\right)\tau'}{1+\omega^2\tau'^2}\right] \quad (5)$$

in which $1/\tau' = 1/\tau_{\mathrm{lipid}} + 1/\tau_{\mathrm{local}}$ was thus used. τ_{local} is the correlation time for the local motion for each measured site and S^2_{local} is the corresponding generalized order parameter squared for the local motion of each site. τ_{lipid} is the correlation time for the reorientation of the lipid molecule within the bicelle and S^2_{lipid} is the generalized order parameter squared for this motion. These dynamic parameters have been determined experimentally for different lipids in bilayers by carbon-13 and deuterium relaxation [35,40,41,68] as well as by EPR [38,39,69]. τ_{lipid} and S^2_{lipid} were therefore kept fixed (to 1.9 ns and to 0.36, respectively) in the final calculation as described previously [35,37]. However, we carefully analyzed the effects of varying these two parameters on the τ_{local} and S^2_{local} parameters (see the Results section). The fitting procedure was performed with the program Matlab (version 7.0) as described previously [35].

Evaluation of the DHPC relaxation data required a little more complicated analysis. Here, it is not reasonable to assume that the overall motion of the DHPC micelle can be neglected. In addition, this overall motion is complicated by the influence of lateral diffusion of individual DHPC molecules. Hence, we used an expression for the spectral density function, which includes three terms according to [68]

$$J(\omega) = \frac{2}{5}\left[\frac{\left(S^2_{\mathrm{lipid}}\tau_{\mathrm{overall}}\right)}{1+\omega^2\tau'^2_{\mathrm{overall}}} + \frac{\left(S^2_{\mathrm{local}} - S^2_{\mathrm{local}}S^2_{\mathrm{lipid}}\right)\tau_{\mathrm{lipid}}}{1+\omega^2\tau^2_{\mathrm{lipid}}} + \frac{\left(1-S^2_{\mathrm{local}}\right)\tau'}{1+\omega^2\tau'^2}\right] \quad (6)$$

in which τ_{overall} is the correlation time for the overall rotation, including lateral diffusion according to $1/\tau_{\mathrm{overall}} = 1/\tau_{\mathrm{rot}} + 1/\tau_{\mathrm{lat}}$, where τ_{rot} is the correlation time for the overall tumbling of the micelle and τ_{lat} is the correlation time for the lateral diffusion of a DHPC molecule (Fig. 1). Several different ways of analyzing the DHPC relaxation data was tested, based on this spectral density function (and of simplifications), and these are described in the Results section. Based on the estimated errors in the relaxation parameters for both DMPC and DHPC, it is judged that the errors in the calculated S^2_{local} are at the most 7%.

3. Results

3.1. Peptide structure

CD spectroscopy was used to investigate the secondary structure of the two peptides in DMPC/DHPC bicelles as well as in POPC vesicles. The two peptides are predicted to be α-helical and it is indeed seen that both peptides are predominantly helical in both media (Fig. 2A). The spectrum of the peptide derived from the HsapBK channel contains also other secondary structures, while the spectrum of the KvAP-derived peptide only contains α-helix and random coil. Both peptides are only marginally soluble in water or buffer, and hence it was difficult to record CD spectra at the same concentrations as in the bicelle solution. However, at lower concentration (100 μM), it was clearly seen that both peptides adopted a random coil structure.

3.2. Acrylamide quenching of Trp fluorescence

The position of the peptides in both bicelles and in vesicles was investigated by intrinsic Trp fluorescence. The sequence corresponding to the paddle domain in KvAP does not contain a Trp, and therefore a construct in which Phe18 was mutated to a Trp was used. The structure of this peptide in bicelles, as judged from CD spectra, did not differ significantly from the KvAPp peptide (data not shown). In the sequence corresponding to the paddle derived from HsapBK, the Trp is located at position 12. Both of these residues are predicted to be located at the turn between helices S3b and S4 [3].

The emission maximum for the Trp in HsapBKp in bicelle solution is at 339 nm, i.e., blue-shifted relative to a Trp in aqueous media, indicating that it is in a more hydrophobic environment (Fig. 2B). For F18W-KvAPp, the emission maximum is at 345 nm, again indicating at least a partial burial of this residue in the hydrophobic interior of a bicelle (Fig. 2B).

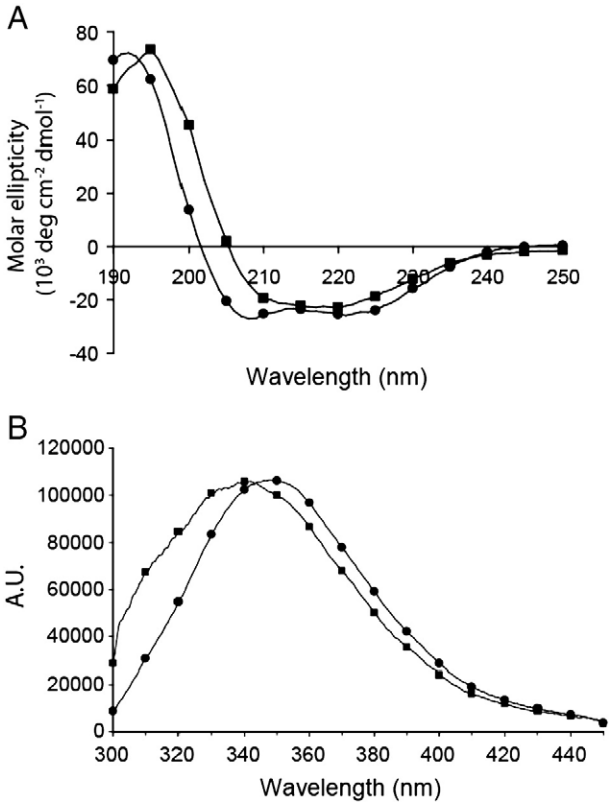

Fig. 2. CD (A) and fluorescence (B) spectra of 0.5 mM KvAPp (circles) and 0.5 mM HsapBKp (squares) in $q = 0.5$ DMPC/DHPC bicelles at 37 °C.

By investigating the effect of the external hydrophilic quencher acrylamide on Trp fluorescence, one can through the Stern-Volmer relationship obtain information about the location of the Trp residues relative to aqueous solution [19]. Stern-Volmer plots for the quenching by acrylamide for the two peptides in DMPC/DHPC bicelles are shown in Fig. 3A. The Stern-Volmer quenching constants are 1.5 M^{-1} and 3 M^{-1} for F18W-KvAPp and HsapBKp, respectively. A Trp residue in water has a quenching constant of around 35 M^{-1}, which indicates that here we see only a very limited amount of quenching. Hence, the Trp residues in both peptides are not exposed to the aqueous solution. The quenching constant for the peptide derived from the HsapBK channel is marginally larger, but is well in the range expected for membrane-inserted Trp residues [70]. The difference may, on the other hand, be due to a slightly more shallow localization of the Trp in HsapBKp as compared to in F18W-KvAPp. We also note that the quenching profile for F18W-KvAPp is not linear, which may indicate non-collisional quenching by the acrylamide [19]. The rates are, however, so low that it is difficult to draw any significant conclusions about this effect.

To compare the bicelles as membrane model for the peptides with a more natural membrane mimetic, large unilamellar vesicles containing POPC lipids were also used for determining Stern-Volmer quenching constants (Fig. 3B). The results were almost identical, indicating that the peptides indeed interact with bicelles in a manner very similar to what they would in LUVs.

3.3. Trp fluorescence quenching by doxyl-labeled lipids

Quenching using phospholipids labeled by a doxyl-group at position 5, 12 or 16 in the acyl chain was also determined (Fig. 4). These probes have been used to give information about the location of Trp residues within lipid bilayers, and it has been demonstrated that a 5-doxyl-labeled stearic acid is localized close to the surface, while the others are more buried in the bilayer [71,72].

The quenching was much more efficient for all doxyl-labels and for both peptides as compared to quenching with acrylamide. For F18W-KvAPp, it was seen that the least amount of quenching was from the 5-doxyl-labeled lipid, with an apparent Stern-Volmer quenching constant of 3.4 mM^{-1}, while the two other lipids had the same effect (K_{SV} = 4.4 mM^{-1}). For HsapBKp, the largest effect was from the 12-doxyl-labeled lipid (K_{SV} = 3.9 mM^{-1}), while, somewhat surprisingly, the result of the 5-doxyl and 16-doxyl-labeled lipids was more similar (K_{SV} = 3.9 mM^{-1} for 5-doxyl and 2.4 mM^{-1} for 16-doxyl-labeled lipid). It has, however, been indicated previously that a great deal of motion in the lipids together with movement of the peptide can result in such observations [58]. The observation may also indicate a more shallow location of the Trp in HsapBKp as compared to KvAPp. This is in agreement with the results from the acrylamide quenching. The parallax method for measuring membrane penetration depth of fluorophores, based on quenching by spin-labeled lipid molecules, can give quantitative information about the insertion depth of a fluorophore (such as the Trp in the peptides) [71,72]. The basic idea is to compare the amount of fluorescence quenching by quenchers located at different positions within a bilayer. In the present case, however, it is not clear what the slight differences in quenching constants are due to, and therefore no attempt was made to evaluate the insertion depth quantitatively.

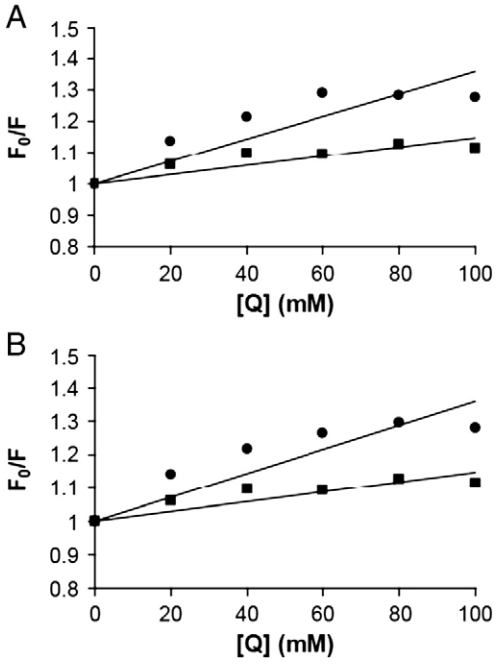

Fig. 3. Stern-Volmer plots for the acrylamide quenching of the Trp fluorescence in KvAPp (circles) and HsapBK (squares). Panel A shows data for the peptides in q = 0.5 DMPC/DHPC bicelles and, panel B shows data for the peptides in large unilamellar POPC vesicles. The peptide concentration was 1.5 mM in bicelles and 50 μM in vesicles. The temperature was 37 °C.

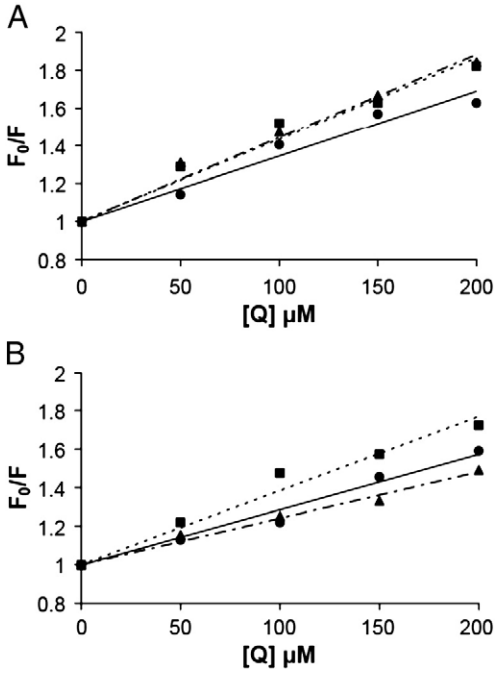

Fig. 4. Stern-Volmer plots for the quenching of the Trp fluorescence by doxyl-labeled POPC in KvAPp (A) and HsapBK (B) in q = 0.5 DMPC/DHPC bicelles. The peptide concentration was 1.5 mM and the temperature was 37 °C. Quenching by 5-doxyl-POPC is indicated by squares, 12-doxyl-POPC by circles and dashed lines and quenching by 16-doxyl-POPC by triangles.

The fluorescence results show that both peptides are embedded within the bilayer of the bicelles, and that slight variations in the location may results in the observed differences in fluorescence quenching. In general, however, the effect of all three lipids was very similar on both peptides. Quenching by doxyl-labeled lipids was investigated also in POPC LUVs, and as for the acrylamide quenching results, very similar data to the ones obtained in bicelles were obtained (data not shown).

3.4. Influence of the peptides on DMPC dynamics

To investigate the effect of the peptides on lipid dynamics, we measured natural abundance carbon-13 nuclear spin relaxation of selected carbons in the DMPC lipids within bicelle bilayers. All carbon (and proton) NMR resonances except those of carbon 2, 3 ,12, 13 and 14 overlap with those of DHPC, and consequently only relaxation data

for carbons in the acyl chain were evaluated. The bicelle size and the DMPC dynamics have been investigated previously in a similar way by pulsed field gradient spin diffusion NMR and by spin relaxation [35].

From R_1 and NOE relaxation data at two fields (9.4 and 14.1 T), we fitted the model-free parameters S^2_{local} and τ_{local} according to Equation (5) for both peptides (see Fig. 1). These parameters are collected in Table 2 and presented in Fig. 5. The order parameters as well as the local correlation times are, as expected, seen to decrease along the acyl chain, [35,37]. Addition of either peptide to the bicelles increases the order parameters for carbons 2 and 3 in the acyl chain (Fig. 5). This is especially valid for carbon 3, indicating that both peptides influence the mobility of the acyl chain within the bilayer. The local correlation times also increase with the addition of either peptide. Again, the most significant effect is observed for carbon 3. These observations indicate that the peptides affect the dynamics of the lipids in the bicelles, making the acyl chains less flexible (higher order parameters) and with slower local motion (longer τ_{local}).

3.5. Influence of the peptides on DHPC dynamics

We also investigated the effect of the two fragments on the lipid head-group mobility. Since the carbon-13 NMR spectrum for DHPC overlaps completely with that of DMPC, we chose DHPC micelles as a membrane mimetic in this case. It is, however, not valid to use the fitting routine that was used for evaluating the relaxation data in bicelles for these relatively small micelles with faster overall motion. To estimate the overall rotational correlation time for a DHPC micelle, we measured the micelle size by dynamic light scattering. The hydrodynamic radius of the micelle showed to be fairly constant over the temperature range of 20–40 °C, and could be estimated to be around 2.2 nm at 37 °C (the temperature at which all relaxation measurements were performed), which is in good agreement with previous results [73,74]. From this value, we can estimate a rotational correlation time of around 5 ns, which is in principle too fast to be neglected in the expression for the spectral density function.

To test if this overall motion has an influence on the spectral density function, and hence the relaxation rates, we calculated $J(\omega)$ for different values of the overall correlation time using Equation (6). First, we calculated the spectral density function at different frequencies using the assumption that the correlation time for the rotational motion of one DHPC molecule within the micelle, τ_{lipid}, and the corresponding order parameter, S^2_{lipid}, is the same as for DMPC (1.9 ns and 0.36, respectively). The order parameter for the local motion was set to $S^2_{\text{local}} = 0.15$. By assuming a long correlation time for the overall motion ($\tau_{\text{overall}} = 100$ ns, as expected for a bicelle), the spectral density function at $\omega = 2\pi \times 125 \times 10^6$ rad s^{-1} (corresponding to the Larmor frequency of carbon at 11.8 T) is $J(\omega) = 0.83 \times 10^{-10}$ s rad^{-1}. Assuming instead a faster overall motion ($\tau_{\text{overall}} = 5$ ns corresponding to that of a DHPC micelle) gives $J(\omega) = 0.93 \times 10^{-10}$ s rad^{-1}. At a higher frequency, corresponding to the highest frequency in the expression for the relaxation rates, $\omega_C + \omega_H = 2\pi \times 625 \times 10^6$ rad s^{-1} at 11.8 T, (see Equation (3)), the spectral density function takes on the value of 0.46×10^{-10} s rad^{-1}, independent of τ_{overall}. This shows that, at low frequencies, the overall motion of the aggregate becomes important in the spectral density function, while at higher frequencies it is not.

Table 2
Model-free parameters[a] for selected carbons in $q = 0.5$ DMPC/DHPC with the addition of KvAPp or HsapBKp.

Carbon[b]	DMPC/DHPC		DMPC/DHPC + KvAPp		DMPC/DHPC + HsapBK	
	S^2_{local}	τ_{local} (ps)	S^2_{local}	τ_{local} (ps)	S^2_{local}	τ_{local} (ps)
2	0.22 ± 0.01	33 ± 3	0.23 ± 0.01	35 ± 5	0.24 ± 0.01	31 ± 3
3	0.12 ± 0.01	19 ± 3	0.16 ± 0.01	28 ± 3	0.14 ± 0.01	30 ± 3
12	0.04 ± 0.01	10 ± 2	0.03 ± 0.01	12 ± 2	0.02 ± 0.01	14 ± 5
13	0.02 ± 0.01	8 ± 2	0.02 ± 0.01	9 ± 2	0.01 ± 0.01	10 ± 2

[a] $S^2_{\text{lipid}} = 0.36$ and $\tau_{\text{lipid}} = 1.9$ ns were kept constant during the fit.
[b] Since the chemical shifts of the *sn1* and *sn2* chains have not been assigned individually, average values are reported.

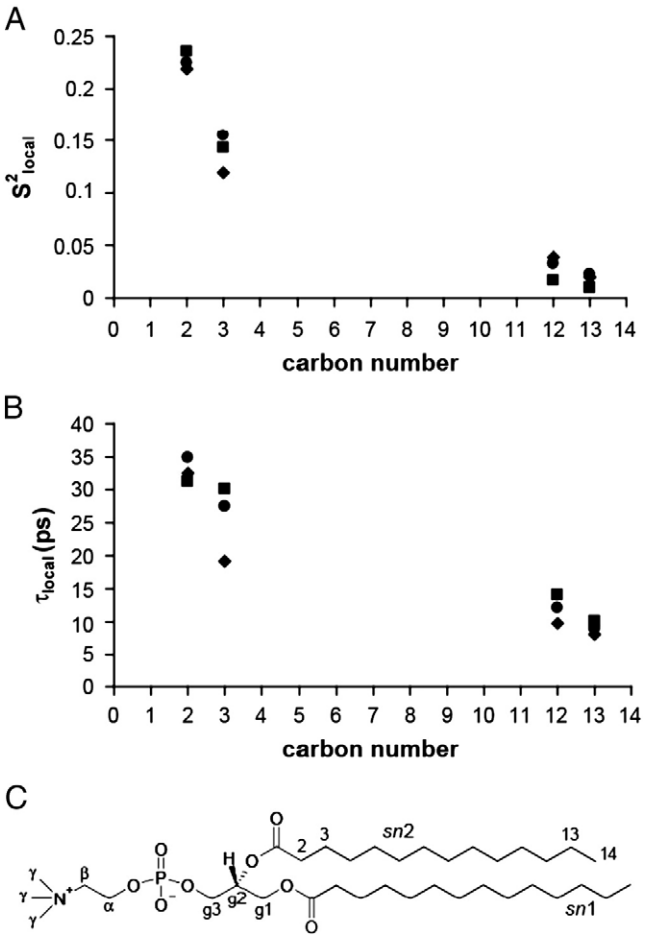

Fig. 5. Generalized order parameter squared, S^2_{local} (A), and local correlation times, τ_{local} (B) for selected positions in the acyl chain for DMPC in $q = 0.5$ bicelles. Order parameters for pure bicelles are shown as diamonds, bicelles with the addition of 3 mM KvAPp as circles and 3 mM HsapBKp as squares. Measurements were performed at 37 °C. Average values for the two chains are reported. Panel C shows the numbering of the carbons in DMPC.

Furthermore, it may not be reasonable to assume that the correlation time for the DHPC rotation, τ_{lipid}, is the same as for DMPC. By assuming a shorter correlation time than what has been determined for DMPC, $\tau_{\text{lipid}} = 1$ or 1.5 ns, in the calculations we, however, get a very similar dependence on the overall motion. In the same way, we varied the S^2_{lipid} parameters to see if this had a great impact on the S^2_{local} parameters. Varying S^2_{lipid} between 0.25 and 0.5 causes a maximum variation of the S^2_{local} parameter of 0.05, and all variations are uniform throughout the DHPC molecule. These calculations show that the spectral density function (and therefore the relaxation rates) depends on the overall motion at low frequencies, hence we have to, in principle, take this motion into account. They also show that modest variations in the motion of the lipid molecule (characterized by τ_{lipid} and S^2_{lipid}) do not influence the interpretation of relaxation rates significantly.

To complicate matters further, the lateral diffusion of individual DHPC molecules in the micelle cannot be neglected. This was shown by Wennerström and co-workers when interpreting relaxation data for octanoate micelles [75]. In their case, the lateral diffusion coefficient for the octanoate molecule was $D = 2 \times 10^{-10}$ m^2 s^{-1}, which corresponds to a rotational correlation time of $\tau_{\text{lat}} = r_h^2/6D = 1.5$ ns. Here, r_h is taken as the hydrodynamic radius of the micelle [75]. For DHPC, we can assume a similar or slower lateral diffusion rate, since this

molecule is slightly larger than the octanoate. Since the correlation times for the overall motion ($\tau_{rot}=5$ ns as determined from DLS), the lipid rotation ($\tau_{lipid}\sim 1$–2 ns estimated from DMPC motion) and the lateral diffusion are on the same time-scale, it is no longer valid to treat them separately. Instead, we may speak about an effective overall correlation time, $1/\tau_{overall}=1/\tau_{rot}+1/\tau_{lipid}+1/\tau_{lat}$. This correlation time can thus be introduced into Equation (5) instead of τ_{lipid}.

Our measurements were made primarily to see how the peptide derived from the two channels influence the local motion of the DHPC (S^2_{local}). To see how different values for τ_{lat} and τ_{lipid} influence the order parameters, S^2_{local}, we fitted the data using three different values for each of the correlation times for the DHPC micelles. The results of these fits are collected in Fig. 6. The results show that no significant variations in the derived order parameters for the local motion was seen for any of the carbons in the DHPC molecule. Hence, the evaluation of the relaxation data for the DHPC molecule could be used with the same parameters as has previously been determined for DMPC.

In this way, we evaluated the relaxation data in terms of S^2_{local} parameters, using the same approach as described for the bicelles. Even if the actual values may be influenced by errors in the assumed dynamics for the entire DHPC molecule, as discussed above, we nevertheless obtain a qualitative estimate of the variation in order parameters with the addition of the peptides.

The S^2_{local} parameters for DHPC with and without the addition of either of the two peptides are collected in Table 3 and shown in Fig. 7. First, we may note that the three glycerol carbons display by far the most restricted motion, with S^2_{local} around 0.5. Interestingly, the highest values are observed for g1, and not g2, which is the most rigid carbon in, for instance DMPC [35]. This may in part be due to the fact that the two chains in DHPC are much shorter, and hence g2 becomes a little more dynamic, while the motion of g1, mainly influenced by the head-group, remains the same. The glycerol carbon–deuterium bond vectors in selectively deuterated DMPC have also been shown, by interpretation of quadrupolar couplings in selectively deuterated DMPC, to be dynamically hindered [76]. The carbons in the acyl chains have on average lower order parameters than the corresponding carbons in DMPC.

We can clearly see that both peptides have a significant influence on the dynamics for the three glycerol carbon–proton vectors, which are already the most dynamically hindered positions in the DHPC molecule. The order parameter square for the three glycerol carbons increases on average from 0.46 to 0.52 upon addition of KvAPp and to 0.53 when adding HsapBKp. Keeping in mind the relatively low amount of peptide to DHPC in the sample (1:70), this is a significant increase in order parameter, comparable to what has previously been observed in peptide-bicelle systems. The effect is much more modest in the choline head-group or in the acyl chains. For HsapBKp, the increase in order parameters for the carbons in the acyl chains (carbons 2 and 3) is somewhat larger than what is seen for KvAPp. These results agree well with the observations for DMPC in the bicelles, i.e., that the peptides have the influence of hindering local mobility close to the head-group.

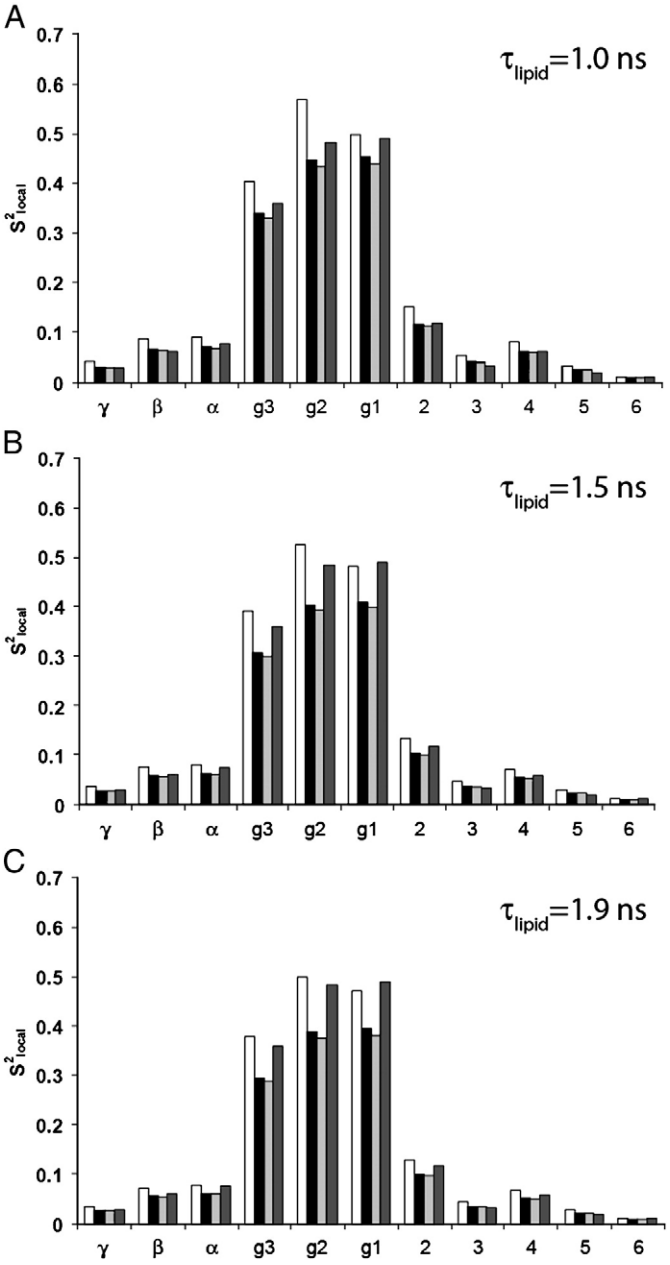

Fig. 6. Effect on the S^2_{local} as a function of varying τ_{lipid} and τ_{lat}. The overall correlation time for the tumbling of the micelle was 5 ns (as determined from DLS). The order parameter for the motion of the DHPC molecule, S^2_{lipid}, was set to 0.36. (A) $\tau_{lipid}=1$ ns; (B) $\tau_{lipid}=1.5$ ns; (C) $\tau_{lipid}=1.9$ ns (as for DMPC). Order parameters were calculated with $\tau_{lat}=1$ ns (white bars), $\tau_{lat}=5$ ns (black bars), $\tau_{lat}=10$ ns (light grey bars) and with the same parameters used for evaluating bicelle relaxation (dark grey bars).

3.6. Influence of the peptides on membrane order—^{2}H NMR

^{2}H NMR spectra were recorded for ^{2}H-labeled DMPC in magnetically aligned $q=3.5$ bicelle mixtures (Fig. 8). The size of the quadrupolar splitting is proportional to the order parameter for the C–^{2}H bond vector of the lipid chain. For pure bicelle mixture, a spectrum with splittings ranging between 2.5 and 20.1 kHz was observed (Fig. 8A). The largest splitting in the spectrum corresponds to the plateau region, which gives the coupling for the C–D vectors closest to the head-group region (the beginning of the acyl chain), and the smallest to the C–D vectors in the methyl groups at the end of the acyl chains [21,22]. It has also been shown by site-specific deuteration that the largest splitting that can be assigned to positions 6 and 7 is the acyl chain [77–79]. In the present case, we focus on the overall changes in the spectra. No major changes are observed in the DMPC spectrum in the presence of KvAPp. The splitting of the outermost peaks is seen to increase slightly (to 20.3 kHz), indicating a minor ordering of the lipid molecules. On the other hand, upon addition of HsapBKp, larger changes in the spectrum are observed. First, the overall appearance of the spectrum changes, indicating that a different phase may be formed. Second, the splittings of the outermost peaks decrease (to 19.3 kHz), indicating a decrease in the order close to the lipid head-group. Hence, the peptide derived from the BK channel appears to change the morphology of the bicelles somewhat. The change in the overall appearance of the spectra upon peptide addition

Table 3
Model-free S^2 parameters[a] for carbons in 200 mM DHPC with the addition of KvAPp or HsapBKp.

Carbon[b]	DHPC	DHPC + KvAPp	DHPC + HsapBK
	S^2_{local}	S^2_{local}	S^2_{local}
γ	0.03 ± 0.01	0.03 ± 0.01	0.03 ± 0.01
β	0.07 ± 0.01	0.06 ± 0.01	0.08 ± 0.01
α	0.08 ± 0.01	0.08 ± 0.01	0.10 ± 0.01
g3	0.37 ± 0.02	0.43 ± 0.03	0.43 ± 0.03
g2	0.49 ± 0.03	0.56 ± 0.04	0.57 ± 0.01
g1	0.50 ± 0.03	0.58 ± 0.04	0.59 ± 0.04
2	0.13 ± 0.01	0.13 ± 0.01	0.16 ± 0.01
3	0.04 ± 0.01	0.04 ± 0.01	0.06 ± 0.01
4	0.06 ± 0.01	0.07 ± 0.01	0.09 ± 0.01
5	0.03 ± 0.01	0.03 ± 0.01	0.03 ± 0.01
6	0.01 ± 0.01	0.01 ± 0.01	0.01 ± 0.01

[a] $S^2_{lipid} = 0.36$ and $\tau_{lipid} = 1.9$ ns were kept constant during the fit.
[b] Since the chemical shifts of the *sn1* and *sn2* chains have not been assigned individually, average values are reported.

could be due to changes in relaxation time constants, indicating that the peptides have an influence on the fast local motion of the C–D bond vectors, in agreement with the present carbon-13 relaxation data [21,80].

The change in the lipid morphology can also be detected by looking at the residual ^2H_2O signal (Fig. 8B). In systems where rapid exchange occurs between water molecules in the partially aligned hydration shell and bulk water, incomplete averaging of the ^2H quadrupole

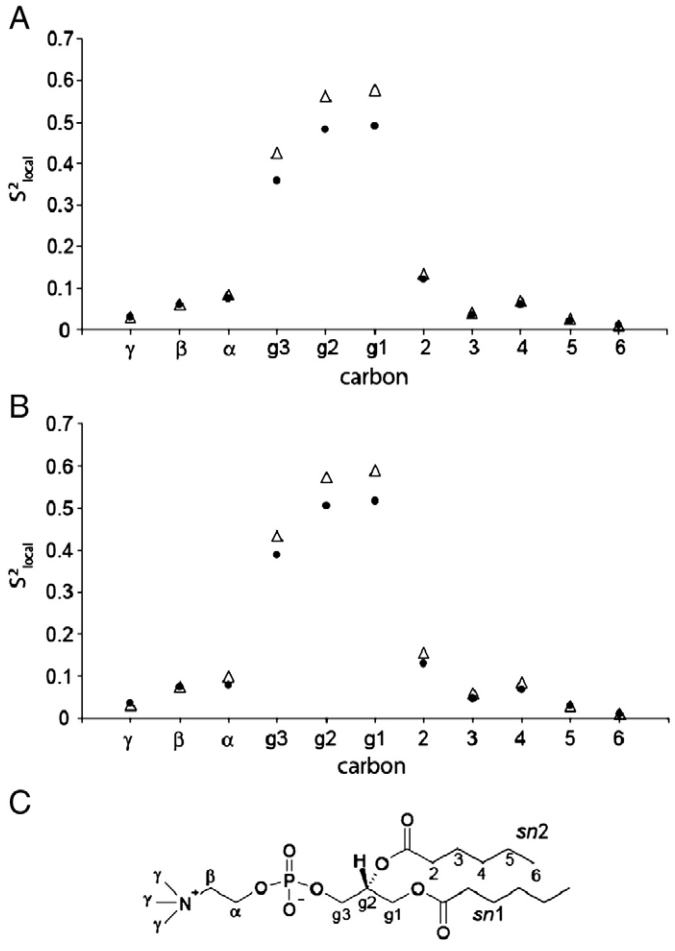

Fig. 7. Generalized order parameter squared, S^2_{local} for carbons in DHPC in 200 mM DHPC micelle solution with and without 3 mM KvAPp (A) and 3 mM HsapBK (B). Closed circles show order parameters for pure DHPC and open triangles show order parameters after the addition of peptide. Panel C shows the numbering of the carbons in DHPC.

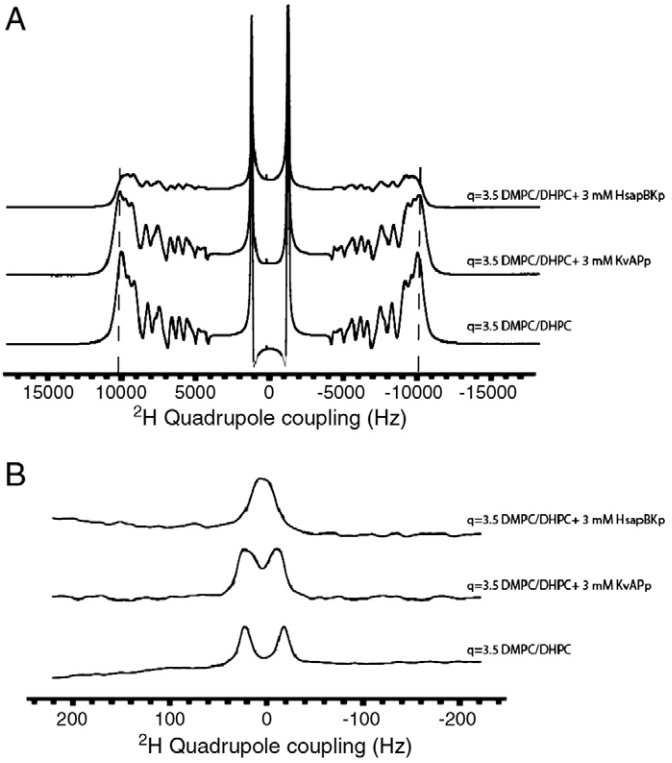

Fig. 8. Deuterium quadrupole echo spectra of magnetically aligned $q = 3.5$ DMPC/DHPC bicelles (bottom spectrum), and of bicelles with 3 mM KvAPp (middle spectrum) or 3 mM HsapBKp (top spectrum) added to the sample. The spectra were recorded at 37 °C. The total lipid concentration was 240 mM. Panel A shows the spectrum for chain-perdeuterated DMPC and panel B shows the spectrum for the residual ^2H_2O signal.

splitting leads to a doublet spectrum [81,82]. In pure bicelles, a doublet signal with a residual quadrupole coupling of 45 Hz is observed. In the presence of KvAPp, this splitting is decreased somewhat, and in the presence of HsapBKp, the splitting is reduced dramatically, indicating that HsapBKp changes the lipid phase, leading to a decrease in the ordering of water molecules, or an increase in the exchange rate between molecules in the hydration shell and the bulk. No isotropic ^2H peak could, however, be observed in the spectrum for chain-deuterated DMPC, which shows that the peptide decreases the order in the bicelles, but does not induce formation of an isotropic phase. Since only small effects on the splittings were observed by adding KvAPp, we draw the conclusion that the two peptides appear to have a different effect on the bilayer stability.

4. Discussion

In this study, we have examined the interaction between two fragments corresponding to the putative "paddle" domains in two different K^+ channels. Both fragments contain Arg residues that are important for the gating of the channels. We wished to examine if these sequences positioned themselves within the bilayer of a bicelle, or if the peptides appear to reside on the surface. The peptides both become helical in the bicelle solvent as indicated by the CD spectra, although other structures seem to be present in the peptide derived from the HsapBK channel.

The fluorescence quenching results show that the Trp residue in either peptide (Trp18 and Trp12 in F18W-KvAPp and HsapBKp, respectively) is not highly exposed to the external aqueous quencher acrylamide, which clearly shows that this part of the peptide is buried within the bilayer, and that it is well separated from the aqueous phase. On the other hand, quenching by 5-, 12-, or 16-doxyl-labeled lipids is more pronounced, demonstrating that both peptide fragments are located within the bilayer. The quenching effect of the three

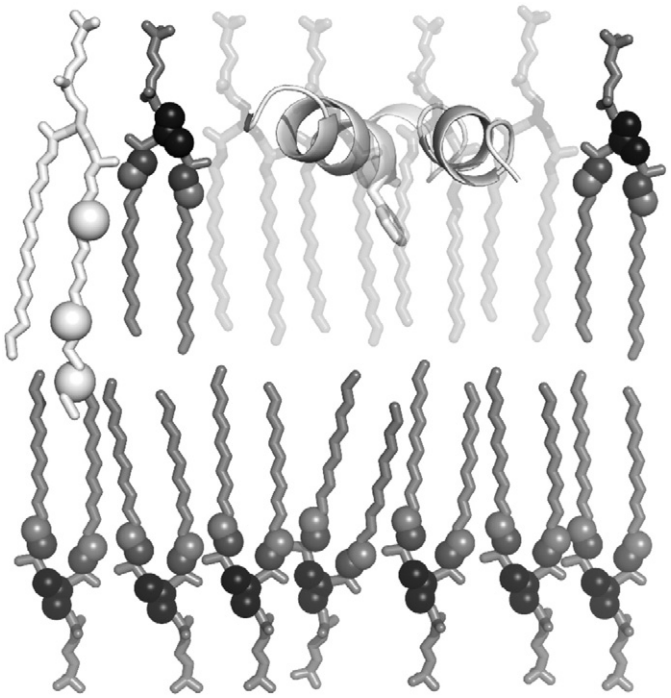

Fig. 9. A model depicting the interaction between HsapBKp and a DMPC bilayer. The doxyl-labels on POPC, used in the fluorescence quenching study, are indicated as white spheres, and the Trp12 side-chain is shown. The glycerol carbons that were most dynamically affected by HsapBKp are shown as black spheres and the C2 and C3 carbons as grey spheres. The figure was generated using PyMol (W.L. DeLano, The PyMol Molecular graphics system (2002), http://www.pymol.org) and the coordinates for the HsapBKp structure were taken from the PDB (www.rcsb.org, accession code 2k44).

different doxyl-labeled lipids is similar, indicating a great deal of mobility of the lipids and peptides. The results also indicate that the peptide derived from the HsapBK channel has a somewhat more shallow localization in the bilayer than the peptide derived from KvAP. It has been demonstrated from biophysical studies of model transmembrane peptides that Trp residues are preferentially located as interfacial anchors in bilayers [83–86]. Our results agree with these observations, although the Trp residue in both fragments seems affected by all doxyl-labeled lipids. Based on the solution NMR structure of HsapBKp [18], a model for how this peptide may be located in a bilayer was made (Fig. 9).

Based on X-ray structures of the KvAP channel and sequence alignments, we anticipate that the Trp residue should be located close to the turn region in both peptides [4,5,8]. The Arg residues are mainly located in the C-terminal part of the sequence (Arg17, Arg20, Arg23, Arg26 and Arg33 in KvAPp and Arg10, Arg16, Arg19 and Arg22 in HsapBKp). However, at least the first two Arg residues in each peptide are close to the Trp, and since the fluorescence data clearly show that the Trp is well protected from aqueous solvent, the results indicate that at least part of the Arg residues appears to be located within the bilayer. It has been demonstrated that the isolated S4 helix from KvAP, containing most of the Arg residues, can be inserted in a membrane in a transmembrane way [87]. Here we demonstrate experimentally that for the fragments corresponding to the "paddle" sequences derived from the two K^+ channels, we see a location within the bilayer. This also demonstrates that the fragments derived from the full-length proteins interact with model membranes as isolated domains and that future investigations of the location of such domains as a function of membrane potential can be carried out in vesicles using, for instance, the approach by Björklund et al. [88].

To study the influence of the fragments on lipid dynamics, we investigated the effect of the peptides on carbon-13 relaxation of lipids in bicelles and of DHPC in micelles. To interpret the data for DHPC, we had to ascertain that the methods by which we evaluate the relaxation data in terms of dynamic parameters are justified. We carefully examined possible effects of various lipid dynamics, such as overall micelle tumbling and lateral diffusion within a micelle, on relaxation and on the fitted dynamic parameters, S^2_{local} and τ_{local}. Our findings show that it is possible to evaluate standard relaxation data for DHPC to yield realistic dynamics parameters. We see that because the order parameters for the carbon–proton vectors in DHPC are relatively low (compared to, e.g., in proteins), the influence of slower micelle tumbling on the spectral density function is limited, which instead is dominated by the local mobility of the carbon–proton bond vectors.

The analysis of the relaxation data shows that both peptides have the effect of making the lipid acyl chains less flexible. This is in agreement with the fluorescence results, again indicating a location of both peptides within the bilayer. Here we do not see a significant difference in the effect of the two peptides. Interestingly, the fragments have the greatest influence on the dynamics of the lipid carbon–proton bond vectors closest to the head-group regions (the glycerol carbons, and carbon 2 and 3 in the acyl chains). This indicates that the sequences interact with the lipids in a way that influences the dynamics of this part of the bilayer, which may be important for sensing the potential, and hence for the movement within the bilayer. In Fig. 9, a model for how HsapBKp interacts with a lipid bilayer is shown, based on both the relaxation data and the fluorescence results. A recent study on lipid dynamics in magnetically aligned bicelles using ^{13}C separated local field NMR spectroscopy showed that the lipid dynamics for the glycerol region in the lipid was very sensitive to different bicelle conditions [89]. This is in agreement with the present findings that the peptides appear to alter the conditions for the glycerol carbons the most.

Both fragments are only marginally soluble in water, which shows that the hydrophobic residues dominate over the charged ones in determining the membrane location. An important difference between the two fragments is that the sequence derived from HsapBK has a significant impact on bilayer integrity and order, while the sequence from KvAP does not appear to have this effect. This, together with the indication that the fragments have slightly different localization within the bilayer, indicates that the voltage sensing may be different. This difference may be related to the fact that the fragments have been taken out of their protein context, but could also be connected to the fact that the predicted paddle domains are very different. The predicted loop region in the KvAP paddle does not appear to be present in the HsapBK-derived paddle [4,5]. Nevertheless, it has been observed that the isolated fragment from HsapBK does indeed form a helix-turn-helix structure in the presence of a bilayer, which is slightly different than what is seen in the X-ray structure of KvAP. Hence, the membrane interaction of the two sensors may differ, indicating that the response to an applied voltage may also differ.

Acknowledgements

We thank Claire Colas for initial CD experiments. This work was supported by grants from the Swedish Research Council, The Center for Biomembrane Research, the Carl Trygger Foundation and the Magnus Bergvall Foundation. A post-doctoral fellowship from the Wenner-Gren Foundation is gratefully acknowledged.

References

[1] F. Bezanilla, The voltage sensor in voltage-dependent ion channels, Physiol. Rev. 80 (2000) 555–592.
[2] F. Bezanilla, Voltage sensor movements, J. Gen. Physiol. 120 (2002) 465–473.
[3] Y. Jiang, V. Ruta, J. Chen, A. Lee, R. MacKinnon, The principle of gating charge movement in a voltage-dependent K channel, Nature 423 (2003) 42–48.

[4] Y. Jiang, A. Lee, J. Chen, M. Cadene, B.T. Chait, R. MacKinnon, The open pore conformation of potassium channels, Nature 417 (2002) 523–526.
[5] Y. Jiang, A. Lee, J. Chen, V. Ruta, M. Cadene, B.T. Chait, R. MacKinnon, X-ray structure of a voltage-dependent K channel, Nature 423 (2003) 33–41.
[6] S.B. Long, E.B. Campbell, R. Mackinnon, Crystal structure of a mammalian voltage-dependent Shaker family K+ channel, Science 309 (2005) 897–903.
[7] S.Y. Lee, A. Lee, J. Chen, R. MacKinnon, Structure of the KvAP voltage-dependent K+ channel and its dependence on the lipid membrane, Proc. Natl. Acad. Sci. U. S. A. 102 (2005) 15441–15446.
[8] S.B. Long, X. Tao, E.B. Campbell, R. MacKinnon, Atomic structure of a voltage-dependent K+ channel in a lipid membrane-like environment, Nature 450 (2007) 376–382.
[9] M. Noda, T. Ikeda, H. Suzuki, H. Takeshima, T. Takahashi, M. Kuno, S. Numa, Expression of functional sodium channels from cloned cDNA, Nature 322 (1986) 826–828.
[10] I.S. Ramsey, M.M. Moran, J.A. Chong, D.E. Clapham, A voltage-gated proton-selective channel lacking the pore domain, Nature 440 (2006) 1213–1216.
[11] M. Sasaki, M. Takagi, Y. Okamura, A voltage sensor-domain protein is a voltage-gated proton channel, Science 312 (2006) 589–592.
[12] A.A. Alabi, M.I. Bahamonde, H.J. Jung, J.I. Kim, K.J. Swartz, Portability of paddle motif function and pharmacology in voltage sensors, Nature 450 (2007) 370–375.
[13] F. Bosmans, M.-F. Martin-Euclaire, K.J. Swartz, Deconstructing voltage sensor function and pharmacology in sodium channels, Nature 456 (2008) 202–208.
[14] K.J. Swartz, Sensing voltage across lipid membranes, Nature 456 (2008) 891–897.
[15] D.J. Posson, P. Ge, C. Miller, F. Bezanilla, P.R. Selvin, Small vertical movement of a K channel voltage sensor measured with luminescence energy transfer, Nature 436 (2005) 848–851.
[16] L.G. Cuello, D.M. Cortes, E. Perozo, Molecular architecture of the KvAP voltage-dependent K+ channel in a lipid bilayer, Science 306 (2004) 491–495.
[17] P. Meera, M. Wallner, M. Song, L. Toro, Large conductance voltage- and calcium-dependent K+ channel, a distinct member of voltage-dependent ion channels with seven N-terminal transmembrane segments (S0–S10) C terminus, Proc. Natl. Acad. Sci. U. S. A. 94 (1997) 14066–14071.
[18] S. Unnerståle, J. Lind, E. Papadopoulos, L. Mäler, Solution Structure of the HsapBK K+ channel voltage-sensor paddle sequence, Biochemistry 48 (2009) 5813–5821.
[19] J.R. Lakowicz, Principles of Fluorescence Spectroscopy, Kluwer Academic, New York, 1999.
[20] J. Seelig, 31P nuclear magnetic resonance and the head group structure of phospholipids in membranes, Biochim. Biophys. Acta 515 (1978) 105–140.
[21] J. Seelig, Deuterium magnetic resonance: theory and application to lipid membranes, Q. Rev. Biophys. 10 (1977) 353–418.
[22] J. Seelig, A. Seelig, Lipid conformation in model membranes and biological membranes, Q. Rev. Biophys. 13 (1980) 19–61.
[23] C.D. Pointer-Keenan, D.K. Lee, K. Hallok, A. Tan, R. Zand, A. Ramamoorthy, Investigation of the interaction of myelin basic protein with phospholipid bilayers using solid-state NMR spectroscopy, Chem. Phys. Lipids 132 (2004) 47–54.
[24] A. Ramamoorthy, S. Thennarasu, A. Tan, D.K. Lee, C. Clayberger, A.M. Krensky, Cell selectivity correlates with membrane-specific interactions: a case study on the antimicrobial peptide G15 derived from granulysin, Biochim. Biophys. Acta 1758 (2006) 154–163.
[25] A. Ramamoorthy, S. Thennarasu, D.K. Lee, A. Tan, L. Maloy, Solid-state NMR investigation of the membrane-disrupting mechanism of antimicrobial peptides MSI-78 and MSI-594 derived from magainin 2 and melittin, Biophys. J. 91 (2006) 206–216.
[26] J.R. Brender, U.H.N. Dürr, D. Heyl, M.B. Budarapu, A. Ramamoorthy, Membrane fragmentation by an amyloidogenic fragment of human islet amyloid polypeptide detected by solid-state NMR spectroscopy of membrane nanotubes, Biochim. Biophys. Acta 1768 (2007) 2026–2029.
[27] M. Ottiger, A. Bax, Characterization of magnetically oriented phospholipid micelles for measurement of dipolar couplings in macromolecules, J. Biomol. NMR 12 (1998) 361–372.
[28] K.J. Glover, J.A. Whiles, G. Wu, N. Yu, R. Deems, J.O. Struppe, R.E. Stark, E.A. Komives, R.R. Vold, Structural evaluation of phospholipid bicelles for solution-state studies of membrane-associated biomolecules, Biophys. J. 81 (2001) 2163–2171.
[29] S.V. Dvinskikh, V. Castro, D. Sandström, Probing segmental order in lipid bilayers at variable hydration levels by amplitude-and phase-modulated cross-polarization NMR, Phys. Chem. Chem. Phys. 7 (2005) 3255–3257.
[30] S. Dvinskikh, U. Dürr, K. Yamamoto, A. Ramamoorthy, A high resolution solid state NMR approach for the structural studies of bicelles, J. Am. Chem. Soc. 128 (2006) 6326.
[31] M. Barry, J.R. Brender, P.E.S. Smith, D.-K. Lee, A. Ramamoorthy, Determining the effects of lipophilic drugs on membrane structure by solid-state NMR spectroscopy: the case of the antioxidant Curcumin, J. Am. Chem. Soc. 131 (2009) 4490–4498.
[32] U.H.N. Dürr, K. Yamamoto, S.-C. Im, L. Waskell, A. Ramamoorthy, Solid-state NMR reveals structural and dynamical properties of a membrane-anchored electron-carrier protein, Cytochrome b_5, J. Am. Chem. Soc. 129 (2007) 6670–6671.
[33] U.H.N. Dürr, L. Waskell, A. Ramamoorthy, The cytochromes P450 and b5 and their reductases – promising targets for structural studies by advanced solid-state NMR spectroscopy, Biochim. Biophys. Acta 1768 (2007) 3235–3259.
[34] P.E.S. Smith, J.R. Brender, A. Ramamoorthy, Induction of negative curvature as a mechanism of cell toxicity by amyloidogenic peptides: the case of Islet amyloid polypeptide, J. Am. Chem. Soc. 131 (2009) 4470–4478.
[35] A. Andersson, L. Mäler, Magnetic resonance investigations of lipid motion in isotropic bicelles, Langmuir 21 (2005) 7702–7709.
[36] A. Andersson, H. Biverståhl, J. Nordin, J. Danielsson, E. Lindahl, L. Mäler, The membrane-induced structure of melittin is correlated with the fluidity of the lipids, Biochim. Biophys. Acta 1768 (2007) 115–121.
[37] J. Lind, J. Nordin, L. Mäler, Lipid dynamics in fast-tumbling bicelles with varying bilayer thickness: effect of model transmembrane peptides, Biochim. Biophys. Acta 1778 (2008) 2526–2534.
[38] J. Freed, New technologies in electron spin resonance, Annu. Rev. Phys. Chem. 51 (2000) 655–689.
[39] Y. Lou, M. Ge, J.H. Freed, A multifrequency ESR study of the complex dynamics of membranes, J. Phys. Chem. B 105 (2001) 11053–11056.
[40] M.F. Brown, A.A. Ribeiro, G.D. Williams, New view of lipid bilayer dynamics from 2H and 13C NMR relaxation time measurements, Proc. Natl. Acad. Sci. U.S.A. 80 (1983) 4325–4329.
[41] M.F. Brown, R.L. Thurmond, S.W. Dodd, D. Otten, K. Beyer, Elastic deformation of membrane bilayers probed by deuterium NMR relaxation, Biochemistry 39 (2000) 1833.
[42] P. Ram, J.H. Prestegard, Magnetic field induced ordering of bile salt/phospholipid micelles: new media for NMR structural investigations, Biochim. Biophys. Acta 940 (1988) 289–294.
[43] C.R. Sanders, J.H. Prestegard, Magnetically orientable phospholipid bilayers containing small amounts of a bile salt analogue, CHAPSO, Biophys. J. 58 (1990) 447–460.
[44] C.R. Sanders, B.J. Hare, K.P. Howard, J.H. Prestegard, Magnetically-oriented phospholipid micelles as a tool for the study of membrane-associated molecules, Prog. NMR Spectrosc. 26 (1994) 421–444.
[45] C.R. Sanders, R.S. Prosser, Bicelles: a model membrane system for all seasons? Structure 6 (1998) 1227–1234.
[46] R.R. Vold, R.S. Prosser, A.J. Deese, Isotropic solutions of phospholipid bicelles: a new membrane mimetic for high-resolution NMR studies of polypeptides, J. Biomol. NMR 9 (1997) 329–335.
[47] P.A. Luchette, T.N. Vetman, R.S. Prosser, R.E.W. Hancock, M.P. Nieh, C.J. Glinka, S. Krueger, J. Katsaras, Morphology of fast-tumbling bicelles: a small angle neutron scattering and NMR study, Biochim. Biophys. Acta 1513 (2001) 83–94.
[48] I. Marcotte, M. Auger, Bicelles as model membranes for solid-and solution-state NMR studies of membrane peptides and proteins, Concepts Magn. Reson. 24 (2005) 17–37.
[49] R.S. Prosser, F. Evanics, J.L. Kitevski, M.S. Al-Abdul-Wahid, Current applications of bicelles in NMR studies of membrane-associated amphiphiles and proteins, Biochemistry 45 (2006) 8453–8465.
[50] C.E. Dempsey, The actions of melittin on membranes, Biochim. Biophys. Acta 1031 (1990) 143–161.
[51] E.J. Dufourc, J.F. Faucon, G. Fourche, J. Dufourcq, T. Gulik-Krzywicki, Le M. Maire, Reversible disk-to-vesicle transition of melittin-DPPC complexes triggered by the phospholipid acyl chain melting, FEBS Lett. 201 (1986) 205–209.
[52] J. Dufourcq, J.F. Faucon, G. Fourche, J.L. Dasseux, T. Gulik-Krzywicki, M. Le Maire, Morphological changes of phosphatidylcholine bilyers induced by melittin: vesicularization, fusion, discoidal particles, Biochim. Biophys. Acta 853 (1986) 33–48.
[53] R. Smith, F. Separovic, F.C. Bennett, B.A. Cornell, Melittin-induced changes in lipid multilayers, a solid-state NMR study, Biophys. J. 63 (1992) 469–474.
[54] R. Smith, F. Separovic, T.J. Milne, A. Whittaker, F.M. Bennett, B.A. Cornell, A. Makriyannis, Structure and orientation of the pore-forming peptide, melittin, in lipid bilayers, J. Mol. Biol. 241 (1994) 456–466.
[55] Y.-H. Lam, S.R. Wassall, C.J. Morton, R. Smith, F. Separovic, Solid-state NMR structure determination of melittin in a lipid environment, Biophys. J. 81 (2001) 2752–2761.
[56] S. Toraya, K. Nishimura, A. Naito, Dynamic structure of vesicle-bound melittin in a variety of lipid chain lengths by solid-state NMR, Biophys. J. 87 (2004) 3323–3335.
[57] L. Mäler, A. Gräslund, Artificial membrane models for the study of macromolecular delivery, Methods Mol. Biol. 480 (2009) 129–139.
[58] P. Damberg, J. Jarvet, A. Gräslund, Micellar systems as solvents in peptide and protein structure determination, Methods Enzymol. 339 (2001) 271–285.
[59] M. Lindberg, A. Gräslund, The position of the cell penetrating peptide penetratin in SDS micelles determined by NMR, FEBS Lett. 497 (2001) 39–44.
[60] M. Lindberg, H. Biverståhl, A. Gräslund, L. Mäler, Structure and positioning comparison of two variants of penetratin in two different membrane mimicking systems by NMR, Eur. J. Biochem. 270 (2003) 3055–3063.
[61] E. Bárány-Wallje, A. Andersson, A. Gräslund, L. Mäler, NMR solution structure and position of transportan in neutral phospholipid bicelles, FEBS Lett. 567 (2004) 265–269.
[62] J.H. Davis, K.R. Jeffrey, M. Bloom, M.I. Valic, Quadrupolar echo deuterium magnetic resonance spectroscopy in ordered hydrocarbon chains, Chem. Phys. Lett. 42 (1976) 390–394.
[63] H. Wennerström, G. Lindblom, B. Lindman, Theoretical aspects on the NMR of quadrupolar ionic nuclei in micellar solutions and amphiphilic liquid crystals, Chem. Scripta 6 (1974) 97–103.
[64] B. Halle, H. Wennerström, Interpretation of magnetic resonance data from water nuclei in heterogeneous systems, J. Chem. Phys. 75 (1981) 1928–1943.
[65] G. Lipari, A. Szabo, Model-free approach to the interpretation of nuclear magnetic resonance relaxation in macromolecules: 1. Theory and range of validity, J. Am. Chem. Soc. 104 (1982) 4546–4559.
[66] G. Lipari, A. Szabo, Model-free approach to the interpretation of nuclear magnetic resonance relaxation in macromolecules: 2. Analysis of experimental results, J. Am. Chem. Soc. 104 (1982) 4559–4570.
[67] H. Wennerström, B. Lindman, O. Söderman, T. Drakenberg, J.B. Rosenholm, Carbon-13 magnetic relaxation in micellar solutions. Influence of aggregate motion on T1, J. Am. Chem. Soc. 101 (1979) 6860–6864.

[68] J.F. Ellena, L.S. Lepore, D.S. Cafiso, Estimating lipid lateral diffusion in phospholipid vesicles from carbon-13 spin-spin relaxation, J. Phys. Chem. 97 (1993) 2952–2957.
[69] L.J. Korstanje, E.E. van Faassen, Y.K. Levine, Reorientational dynamics in lipid vesicles and liposomes studied with ESR: effects of hydration, curvature and unsaturation, Biochim. Biophys. Acta 982 (1989) 196–204.
[70] M. Magzoub, K. Kilk, L.E. Eriksson, Ü. Langel, A. Gräslund, Interaction and structure induction of cell-penetrating peptides in the presence of phospholipid vesicles, Biochim. Biophys. Acta 1512 (2001) 77–89.
[71] A. Chattopadhyay, E. London, Parallax method for direct measurement of membrane penetration depth utilizing fluorescence quenching by spin-labeled phospholipids, Biochemistry 26 (1987) 39–45.
[72] F.S. Abrams, E. London, Extension of the parallax analysis of membrane penetration depth to the polar region of model membranes: use of fluorescence quenching by a spin-label attached to the phospholipid polar head group, Biochemistry 32 (1993) 10826–10831.
[73] J.J. Chou, J.L. Baber, A. Bax, Characterization of phospholipid mixed micelles by translational diffusion, J. Biomol. NMR 29 (2004) 299–308.
[74] L. van Dam, G. Karlsson, K. Edwards, Direct observation and characterization of DMPC/DHPC aggregates under conditions relevant for biological solution NMR, Biochim. Biophys. Acta 1664 (2004) 241–256.
[75] H. Wennerström, B. Lindman, Micelles, physical chemistry of surfactant association, Phys. Rep. 52 (1979) 1–86.
[76] L. Strenk, P.W. Westerman, J.W. Doane, A model of orientational ordering in phosphatidylcholine bilayers based on conformational analysis of the glycerol backbone region, Biophys. J. 48 (1985) 765–773.
[77] A. Seelig, J. Seelig, The dynamic structure of fatty acyl chains in a phospholipid bilayer measured by deuterium magnetic resonance, Biochemistry 13 (1974) 4839–4845.
[78] E. Oldfield, M. Meadows, D. Rice, R. Jacobs, Spectroscopic studies of specifically deuterium labelled membrane system. Nuclear magnetic resonance investigation of the effects of cholesterol in model systems, Biochemistry 17 (1978) 2727–2740.
[79] J.A. Urbina, S. Pekerar, H. Le, J. Patterson, B. Montez, E. Oldfield, Molecular order and dynamics of phosphatidylcholine bilayer membranes in the presence of cholesterol, ergosterol and lanosterol: a comparative study using 2H-, 13C-and 31P-NMR spectroscopy, Biochim. Biophys. Acta 1238 (1995) 163–176.
[80] J.D. Gehman, F. Luc, K. Hall, T.-H. Lee, M.P. Boland, T.L. Pukala, J.H. Bowie, M.-I. Aguilar, F. Separovic, Effect of antimicrobial peptides from Australian tree frogs on anionic phospholipid membranes, Biochemistry 47 (2008) 8557–8565.
[81] N.J. Salsbury, A. Darke, D. Chapman, Deuteron magnetic resonance studies of water associated with phospholipids, Chem. Phys. Lipids 8 (1972) 142–151.
[82] E.G. Finer, A. Darke, Phospholipid hydration studied by deuteron magnetic resonance spectroscopy, Chem. Phys. Lipids 12 (1974) 1–16.
[83] J.A. Killian, I. Salemink, M.R.R. de Planque, G. Lindblom, R.E. Koeppe II, D.V. Greathouse, Induction of nonbilayer structures in diacylphosphatidylcholine model membranes by transmembrane α -helical peptides: importance of hydrophobic mismatch and proposed role of tryptophans, Biochemistry 35 (1996) 1037–1045.
[84] M.R.R. de Planque, J.-W.P. Boots, D.T.S. Rijkers, R.M.J. Liskamp, D.V. Greathouse, J.A. Killian, The effects of hydrophobic mismatch between phosphatidylcholine bilayers and transmembrane α -helical peptides depend on the nature of interfacially exposed aromatic and charged residues, Biochemistry 41 (2002) 8396–8404.
[85] M.R. de Planque, J.A. Killian, Protein-lipid interactions studied with designed transmembrane peptides: role of hydrophobic matching and interfacial anchoring, Mol. Membr. Biol. 20 (2003) 271–284.
[86] M.R. de Planque, B.B. Bonev, J.A. Demmers, D.V. Greathouse, R.E. Koeppe, F. Separovic, A. Watts, J.A. Killian, Interfacial anchor properties of tryptophan residues in transmembrane peptides can dominate over hydrophobic matching effects in peptide-lipid interactions, Biochemistry 42 (2003) 5341–5348.
[87] T. Hessa, S.H. White, G. Von Heijne, Membrane insertion of a potassium-channel voltage sensor, Science 307 (2005) 1427.
[88] J. Björklund, H. Biverståhl, A. Gräslund, L. Mäler, P. Brzezinski, Real-time transmembrane translocation of penetratin driven by light-generated proton pumping, Biophys. J. 91 (2006) 29–31.
[89] K. Yamamoto, R. Soong, A. Ramamoorthy, Comprehensive analysis of lipid dynamics variation with lipid composition and hydration of bicelles using nuclear magnetic resonance (NMR) spectroscopy, Langmuir 25 (2009) 7010–7018.